Removal of Basic Orange 2 dye and Ni^{2+} from aqueous solutions using alkaline-modified nanoclay

Armin Geroeeyan, Ali Niazi and Elaheh Konoz

ABSTRACT

In the present research, the removal of Basic Orange 2 (BO2) dye using alkaline-modified clay nanoparticles was studied. To characterize the adsorbent, XRD, FTIR, FESEM, EDX, BET and BJH analyses were performed. The effect of the variables influencing the dye adsorption process such as adsorbent dose, contact time, pH, stirring rate, temperature, and initial dye concentration was investigated. Furthermore, the high efficiency of Ni^{2+} removal indicated that it is possible to remove both dye and metal cation under the same optimum conditions. The experimental data were analyzed by Langmuir and Freundlich isotherm models. Fitting the experimental data to Langmuir isotherm indicated that the monolayer adsorption of dye occurred at homogeneous sites. Experimental data were also analyzed with pseudo-first-order, pseudo-second-order, and intra-particle diffusion kinetic equations for kinetic modeling of the dye removal process. The adsorption results indicated that the process follows a pseudo-second-order kinetic model. The thermodynamic parameters of the dye adsorption process such as enthalpy, entropy, and Gibbs free energy changes were calculated and revealed that the adsorption process was spontaneous and endothermic in nature. The results presented the high potential of the modified nanoclay as a cost-effective adsorbent for the removal of BO2 dye and Ni^{2+} from aqueous medium.

Key words | adsorption, kinetics, nanoclay, removal, surface modification, thermodynamics

Armin Geroeeyan
Department of Chemistry,
Arak Branch, Islamic Azad University,
Arak,
Iran

Ali Niazi (corresponding author)
Elaheh Konoz
Department of Chemistry,
Central Tehran Branch, Islamic Azad University,
Tehran,
Iran
E-mail: *ali.niazi@gmail.com*

HIGHLIGHTS

- The decolorization kinetics of BO2 was followed by a pseudo-second-order kinetic model.
- The adsorption of BO2 was spontaneous and endothermic.
- The efficiency of Ni^{2+} removal confirmed the possibility of the removal of BO2 dye and Ni^{2+} simultaneously under optimum conditions.
- The modified nanoclay can be a potential candidate for removing BO2 dye and Ni^{2+} from textile wastewater.

doi: 10.2166/wst.2021.121

GRAPHICAL ABSTRACT

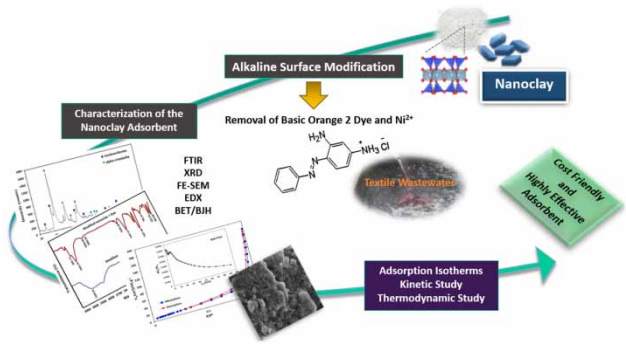

INTRODUCTION

Releasing industrial wastewaters containing heavy metals such as lead, copper, nickel, cobalt, and chromium, as well as dyes from the textile, cosmetics, pharmaceutical, paper, paint, printing, and ink industries to surface waters and the surrounding environment has become a severe problem for the ecosystem and human health (Senthilkumaar *et al.* 2005; Banerjee *et al.* 2014; Gunatilake 2015). It is estimated that about 700,000 tons of dyes are produced annually in the chemical industry worldwide, and about 10–15% of dye-containing effluents are released into the environment (Gamoudi & Srasra 2019).

Generally, dyes as organic pollutants have a synthetic origin and are characterized by complex aromatic molecular structures and high physicochemical, thermal, and optical stability. Basic dyes are cationic dyes and are widely used in various industries. These dyes are commonly applied in the paper, pharmaceutical industries, and dyeing of polyester and nylon fibers in textile industries (Pimol *et al.* 2008; Salleh *et al.* 2011). Because of these features, dye-containing contaminations cause many environmentally severe problems according to their low biodegradability characteristics, and toxicity to aquatic life, and the conventional biological treatment procedures are not efficient enough to treat wastewaters. (Padmesh *et al.* 2005; Ong *et al.* 2007; Soltani *et al.* 2013). Heavy metals as inorganic pollutants, as in dyes, are also highly resistant to environmental degradation, and can damage body organs due to their carcinogenic and mutagenic effects on humans and other organisms depending on dose and duration of exposure (Khataee *et al.* 2013; Kumar *et al.* 2013). High concentrations of nickel as a heavy metal can cause serious health effects due to its numerous applications in various industries including battery, stainless steel, galvanization, electroplating, printing, and pigment industries (Cempel & Nikel 2006; Malayoglu 2018). Therefore, uncontrolled discharge of colored water and solutions containing dyes and toxic heavy metals from industries produce large quantities polluted waters and with due attention to the potentially harmful effects of such compounds on the environment and humans, they must be removed from wastewaters before discharging into the surrounding environment (Mahdavinia *et al.* 2012).

Various treatment methods including physical, chemical, and biological methods such as membrane processes, adsorption, ion exchange, chemical precipitation, chemical and electrochemical oxidation and advanced oxidation by homogeneous and heterogeneous photocatalysts, activated sludge, and anaerobic processes have been applied for the removal and degradation of organic pollutants (Gunatilake 2015; Xiao *et al.* 2015; Haddad *et al.* 2018; Li *et al.* 2018; Sharifi *et al.* 2019). Among these techniques, adsorption was found as a promising way for hazardous pollutants removal from wastewaters due to the advantages of its simple operation, effectiveness, high treatment efficiency, and applicability for the removal of various types of pollutants such as dyes and heavy metals. (Yagub *et al.* 2014; Adeyemo *et al.* 2017; Wang *et al.* 2018). Given these explanations, adsorption is the most preferred technique that has been widely applied as the economic and efficient physicochemical process for the treatment of polluted wastewaters containing dyes, heavy metals, and other organic and inorganic contaminants (Almeida *et al.* 2009).

Activated carbon has been known as the most commonly used adsorbent in the adsorption process because of its high capacity for the adsorption of organic pollutants

and heavy metals (Mezohegyi *et al.* 2012). However, the application of activated carbon is limited due to its cost-prohibitive and regeneration problems (Beyene 2014). To overcome these limitations, research studies have focused on low-cost adsorbents. Clay mineral adsorbents are the promising alternative to activated carbon and have been extensively considered for water purification and wastewater treatments (El-Geundi 1997; Park *et al.* 2011; Jiang & Ashekuzzaman 2012). Clay minerals are available naturally that have drawn attention according to their specific characteristics: availability, environmentally friendliness, cost-effectiveness, high chemical and mechanical stability, and large surface area. Also, they are widely used to substitute the expensive commercial activated carbon in various treatment processes because of their high adsorption capacity due to more active sites on the surface, ion exchangeable and non-toxic properties (Murray 2000; Adeyemo *et al.* 2017; Uddin 2017). The performance of clay minerals to remove harmful materials is due to the space between their layers, and the negative surface charges of their structures allow them to adsorb positively charged dyes and heavy metals (Öztürk & Malkoc 2014; Uddin 2017).

Nanoclays belong to the extensive group of clay minerals are known as the nanoparticles of layered mineral silicates that have received much attention according to the cost efficiency, high surface reactivity, and easy modification procedures. The modification of the surface of nanoclays through diverse procedures provides tremendous scope to make more improvements to the properties of clays (Nazir *et al.* 2016). Raw and modified nanoclay adsorbents have been successfully applied for the removal of a variety of dyes (Auta & Hameed 2012; Ehsan *et al.* 2017; Salam *et al.* 2017; El Haouti *et al.* 2019; Mahvi & Dalvand 2020) and heavy metals (Ren *et al.* 2014; Zhu *et al.* 2019). Basic Orange 2 dye (BO2: which is also known as Chrysoidine) is an example of a cationic dye that is widely used in the textile industries (Qamar *et al.* 2005). The adsorption of BO2 dye from aqueous medium has been reported using amino ethyl-functionalized SBA-15 (AEF-SBA-15) as the adsorbent (Hajiaghababaei *et al.* 2017). In another study, poly-γ-glutamic acid (PGA) biosorbent was used to scrutinize the mechanisms of BO2 dye removal (Hisada *et al.* 2019). There has been no report based on the alkaline modification of nanoclay mineral adsorbent to the best of our knowledge for the removal of BO2 dye.

In the present study, the removal of synthetic Basic Orange 2 dye from aqueous solutions was studied using an alkaline-modified clay nano-adsorbent. In particular, the novelty of this research lies in applying alkaline-modified nanoclay with specific physicochemical properties that have been demonstrated to be a cost-friendly, highly effective, and widely available material in the treatment of aqueous solutions. A simple procedure was required for the modification process that was not time-consuming and did not need any corrosive material and high temperature for treatment of the nanoclay. The effects of important variables on the adsorption efficiency, including adsorbent dose, contact time, pH, stirring rate, temperature, and initial dye concentration, were investigated. Furthermore, the removal of Ni^{2+} heavy metal was evaluated under optimum conditions of BO2 dye adsorption. To examine the adsorption mechanism, equilibrium data were analyzed with relevant isotherms and kinetic models. Also, thermodynamic parameters like change in Gibbs free energy, enthalpy, and entropy for the removal process were determined and described. The results presented the high potential of modified nanoclay, which can be applied as a feasible approach to removing BO2 dye and Ni^{2+} from textile wastewater.

MATERIALS AND METHODS

Preparation of stock solution

Nanoclay as an inorganic adsorbent was purchased from Tamad Kala (Iran) and was applied to remove organic and inorganic pollutants. Sodium hydroxide (NaOH) and hydrochloric acid (HCl) were also purchased from Merck (Darmstadt, Germany) and applied at the concentration of 1 mol L^{-1} to adjust the pH of the solutions. Likewise, sodium hydroxide at a concentration of 1 mol L^{-1} was used for surface modification of the mineral nano-adsorbent. Basic Orange 2 (BO2), as a basic and cationic dye with high purity and in the role of adsorbate, was supplied by Alvan Sabet (Iran) and was not purified prior to use. Some of the physical and chemical characteristics of BO2 dye are given in Table 1. $Ni(NO_3)_2.10H_2O$ with high purity was purchased

Table 1 | Physical and chemical properties of BO2 dye

Chemical formula	$C_{12}H_{13}ClN_4$
Molecular weight	248.71 g mol^{-1}
Density	1–1.1 g cm^{-3}
Chemical structure	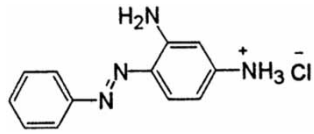

from Merck and used for the preparation of solutions containing Ni^{2+}. The stock solutions of BO2 dye and Ni^{2+} at a concentration of 1000 mg L^{-1} were prepared by weighing and dissolving the corresponding compounds in deionized water. The working solutions were then made by dilution of stock solutions with deionized water to obtain the various initial concentrations for the experiments.

Preparation of the alkaline-modified nanoclay adsorbent

For the alkaline surface modification of the nanoclay adsorbent, the amount of 25 g of nanoclay was added to 250 ml of 1 M NaOH solution and refluxed at 80 °C for 2 h. The prepared solution was cooled at ambient temperature for 24 h, and then filtered to separate the nanoclay adsorbent from the solution. The processed nanoclay was washed three times with deionized water and then dried in an oven at 120 °C for 4 hours. The final sample was stored in a vial for further experiments and used as the modified nanoclay adsorbent to remove BO2 dye and Ni^{2+}.

Adsorption experiments

The adsorption experiments were carried out through a batch operational system (Jar-test apparatus, model FC6S, Velp Scientifica) to investigate the performance of the modified nanoclay absorbent and determine the optimum experimental conditions for removal of BO2 dye and Ni^{2+}. For this purpose, solutions containing each of the pollutants were prepared in various initial concentrations and followed by adding different amounts of the adsorbent (0.02–0.08 g L^{-1}) to the solutions. The mixture was agitated for different times at room temperature with a magnetic stirrer. After achieving steady-state adsorption in the experiment, the adsorbent was separated from the solution by centrifugation at 10,000 rpm (Hettich, Universal 320) for 10 min and the supernatant was extracted. The residual dye and heavy metal concentrations were measured using a UV-Vis spectrophotometer (Lambda 25, Perkin Elmer) for BO2 dye ($\lambda_{max} = 453$ nm) and an atomic absorption spectrophotometer (PG 990 model) for Ni^{2+}.

Various experimental variables such as adsorbent dose, contact time, pH, stirring rate, temperature, and initial dye concentration were investigated. The removal percentages ($R\%$) of BO2 dye and Ni^{2+} from aqueous solutions and the value of adsorption capacity were calculated through Equations (1) and (2):

$$\% R = \frac{(C_o - C_e)}{C_o} \times 100 \quad (1)$$

$$q_e = \frac{(C_o - C_e)V}{m} \quad (2)$$

where C_o and C_e (mg L^{-1}) are initial and equilibrium concentrations of BO2 dye and Ni^{2+} respectively, q_e (mg g^{-1}) represents the adsorption capacity, V (L) is the volume of solution, and m (g) is the adsorbent dose value.

Characterization of adsorbent

To identify the adsorbent functional groups and verify dye adsorption onto the modified nanoclay surface, Fourier transform infrared (FTIR) spectra of samples were recorded using a Thermo Nicolet Avatar 380 spectrometer in the range 400–4,000 cm^{-1}. The surface morphology and porosity of the modified nanoclay, Ni^{2+} and dye-loaded modified nanoclay were examined by field emission scanning electron microscopy (FESEM) (TESCAN, MIRA3). The elemental composition of the modified nanoclay before and after the adsorption of dye and heavy metal was provided by energy-dispersive X-ray spectroscopy (EDX) analysis (SAMx, France). X-ray diffraction (XRD) measurement of the adsorbent was performed using a PW1730 diffractometer (PHILIPS, The Netherlands) with a Cu-Kα radiation ($\lambda = 0.154056$ nm) at 30 kV and 40 mA. The diffraction pattern was recorded by step scanning from 10° to 80° (2θ) at a scan speed of 0.05°/step and 1 s/step. Brunauer–Emmett–Teller (BET) analysis (Belsorp mini II BEL, Japan) was carried out to evaluate the specific surface area of the adsorbent from N_2 adsorption–desorption isotherms at 77 K. The Barrett–Joyner–Halenda (BJH) method was applied to obtain the pore size distribution of the adsorbent.

RESULTS AND DISCUSSION

Characterization of the adsorbent

X-ray analysis

X-ray diffraction measurement was employed to study the crystalline structure and size of nanoclay crystals. As demonstrated in Figure 1, the XRD pattern of the adsorbent

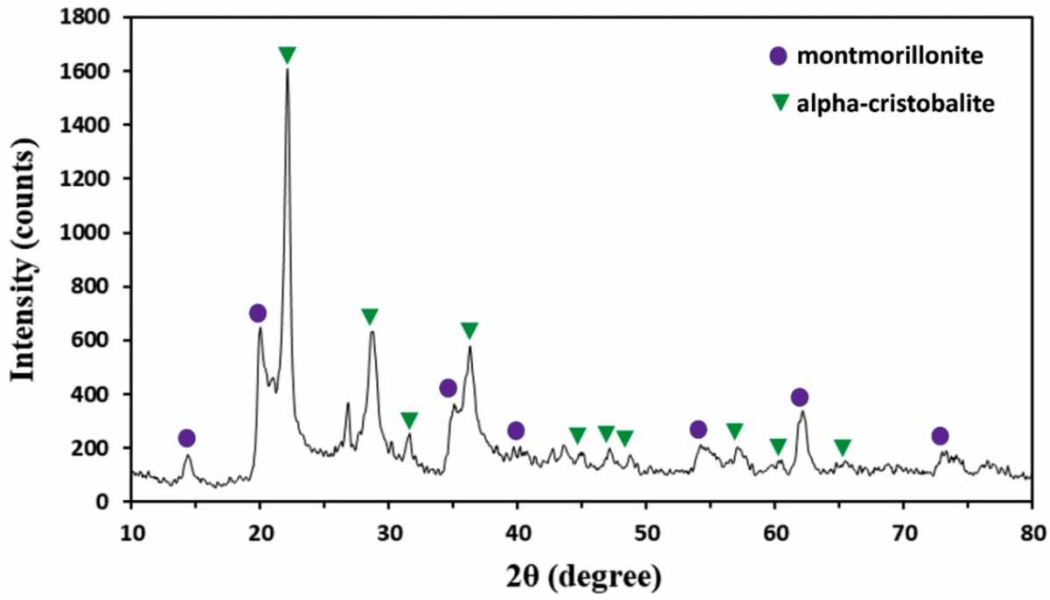

Figure 1 | XRD pattern of the adsorbent.

showed that nanoclay is mainly composed of montmorillonite ($AlSi_2O_6(OH)_2$) mineral with alpha-cristobalite (SiO_2). The sharp and clear reflections of the pattern indicated that the adsorbent has a crystalline structure in nature. The characteristic peak of the montmorillonite at $2\theta = 14.46^\circ$ corresponds to the interlayer spacing of 6.12 Å. Furthermore, montmorillonite represented the diffraction peak at 2θ of 14.46°, 20.26°, 35.12°, 40.23°, 54.71°, 62.16°, and 73.53°. The other diffraction peaks correspond to alpha-cristobalite and other impurities. The average crystallite size of the adsorbent was calculated using the Debye–Scherrer equation $d = (k\lambda/\beta\cos\theta)$, where d is the crystalline size (nm), λ is the wavelength of the Cu-Kα X-ray radiation (0.154056 nm), k is the equation constant (0.9), β is the full width at half maximum (FWHM), and θ is the diffraction angle of the reflection (Hassani *et al.* 2016). The analyses of the XRD pattern using the known Debye–Scherrer equation designated that the average particle size for the interlayer spacing of nanoclay crystals was obtained to be about 16.50 nm.

FTIR analysis

The FTIR spectra of the modified nanoclay before and after the adsorption of BO2 are shown in Figure 2. The bands at 1,027.05 and 1,021.46 cm^{-1} were attributed to the stretching vibrations of Si–O groups. The broad absorption bands in the region between 3,000 and 3,600 cm^{-1} were allocated to the stretching vibration of the hydroxyl groups (O–H) and the stretching vibrations of the intra-layer of the water molecules.

Moreover, the band at around 1,658.64 cm^{-1} was related to bending vibrations of H–O–H groups of water molecules adsorbed on nanoclay structure. The bands observed in the areas at 908.78 and 864.00 cm^{-1} were related to the bending vibrations of the Al–Al–OH and Al–Mg–OH groups at the nanoclay edges (Djomgoue & Njopwouo 2013). The bending vibrations of Si–O–Al and Si–O–Si groups were observed at around 521.15 and 463.92 cm^{-1}, respectively (Alexandre & Dubois 2000; Djomgoue & Njopwouo 2013; Fil *et al.* 2014). The absorption peaks in the 1,440–1,450 cm^{-1} range can be associated with the presence of carbonates (Ouaddari *et al.* 2019). After the adsorption of dye onto the modified nanoclay surface, absorption bands appeared at around 3,551.73 and 3,463.76 cm^{-1} and were related to the vibrational bond of the N–H groups of the BO2 dye molecule and hydroxyl stretching vibrations (Vanamudan & Pamidimukkala 2015). The bands exhibited at 2,926.09 and 2,856.26 cm^{-1} were attributed to the asymmetric and symmetric stretching vibrations of CH_2 groups, respectively. Also, the bands at about 1,639.35 cm^{-1} could be assigned to the aromatic stretching vibration of C=C of BO2 dye (Anirudhan & Ramachandran 2015). It is highlighted that the shift of bands and/or change in the intensities of Si–O and all of O–H vibrations could be related to the strong electrostatic interactions and the hydrogen bonds between these functions and dye, indicating that dye molecules are well adsorbed by modified nanoclay (El Haouti *et al.* 2019).

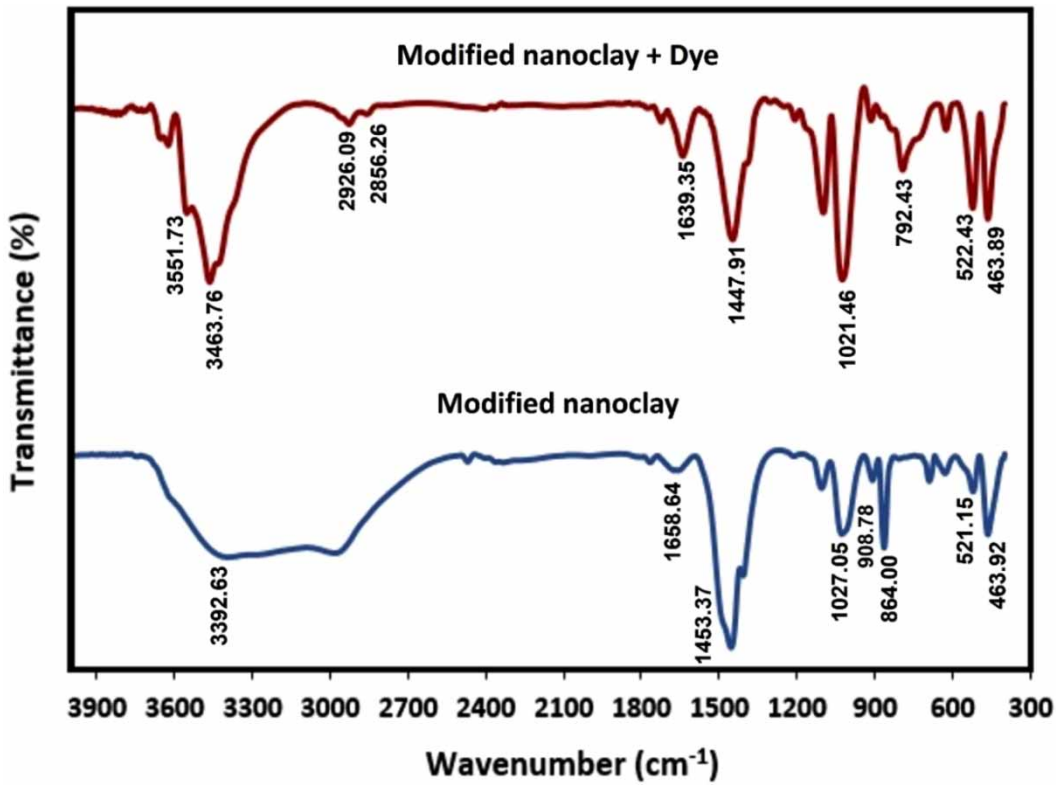

Figure 2 | FTIR spectrum of modified nanoclay before and after the adsorption of BO2 dye.

Morphological analysis

To investigate the surface morphology of the adsorbent, FESEM images of the surface-modified nanoclay, BO2 dye, and Ni^{2+} loaded adsorbent are presented in Figure 3(a)–3(c). As can be seen in Figure 3(a), the adsorbent has heterogeneous porosity and a rough surface, indicating that the adsorbent can adsorb dye molecules through a diffusion process. After BO2 dye adsorption, the uniformity of the surface showed that the compounds were adsorbed onto the nanoclay surface (Figure 3(b)). Moreover, the FESEM images of the adsorbent after adsorption of dye molecules and Ni^{2+} as organic and inorganic pollutants are shown in Figure 3(c), which also indicated that the more porous nature of alkaline-modified nanoclay enhanced the adsorption potential for both dye and metal cations.

EDX analysis

EDX analysis evaluates the elemental composition of the adsorbents before and after the adsorption process (Rao & Kashifuddin 2016; Batista *et al.* 2017). Based on the EDX micrographs, the major portion of the adsorbent was composed of Si, O, Al, and Mg elements (Figure 4(a)–4(c)) showed the agreement with XRD and FTIR results, which revealed that the nanoclay was formed from montmorillonite and alpha-cristobalite minerals. The presence of Ni^{2+} as adsorbate onto the surface of modified nanoclay was confirmed by the Ni element (Figure 4(b) and 4(c)). From the EDX spectra of BO2 loaded modified nanocaly in Figure 4(a), it is demonstrated that BO2 dye consists of specific elements such as C and N. The appeared peaks of C, N, and Cl after the dye adsorption process confirmed the successful adsorption of BO2 dye onto the surface of modified nanoclay.

BET and BJH analysis

The N_2 adsorption–desorption isotherms and the pore size distribution of the adsorbent were estimated using BET and BJH analysis. The BET surface area of the adsorbent was conducted at 77 K. As shown in Figure 5, the adsorbent represented an isotherm of Type IV and H3 hysteresis loop features according to the IUPAC classification system. The type H3 hysteresis loop is typically in aggregates of plate-like particles consisting of slit-shaped pores. The Type IV

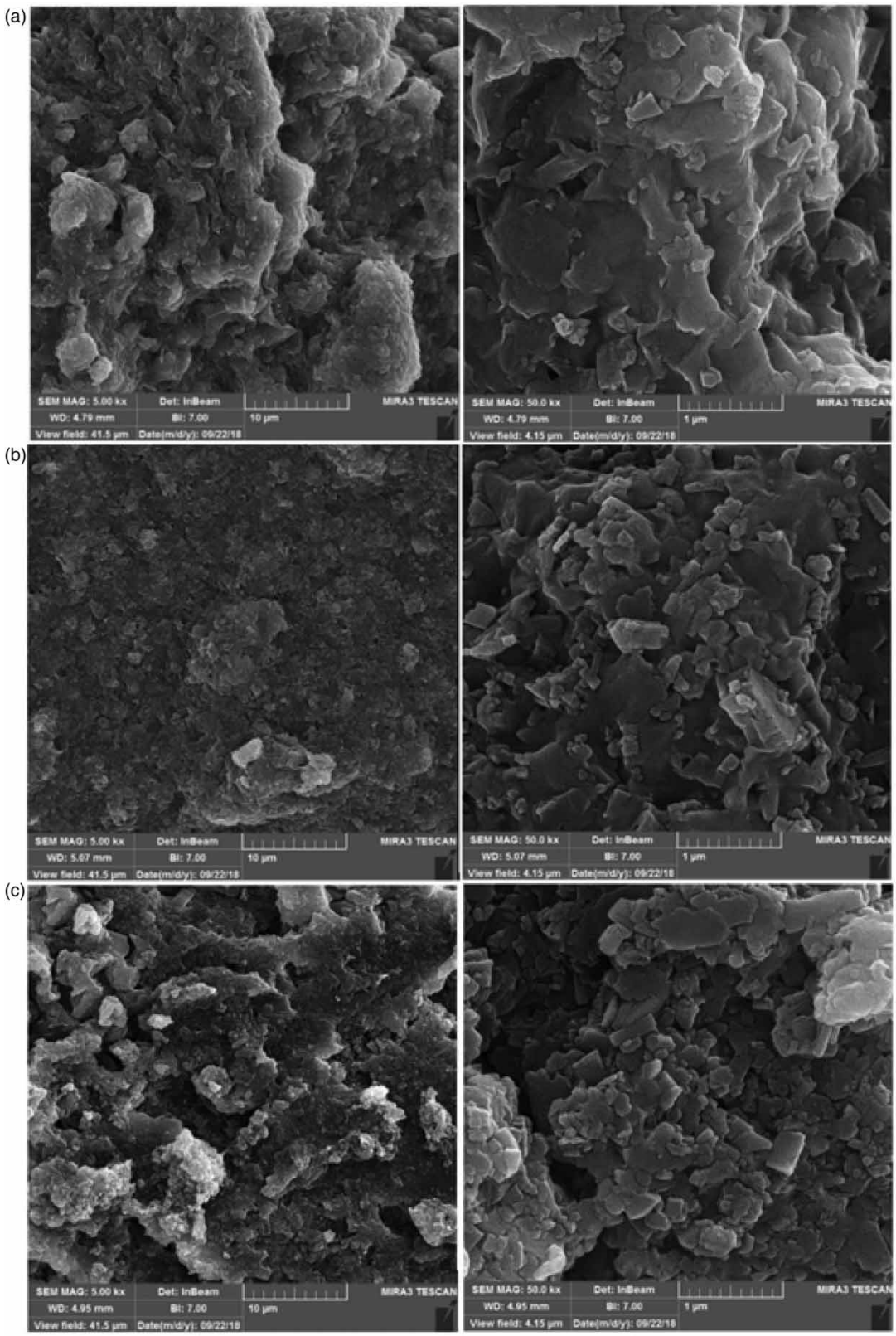

Figure 3 | FESEM images of (a) the modified nanoclay, (b) BO2 dye-loaded, and (c) BO2 and Ni^{2+} loaded modified nanoclay.

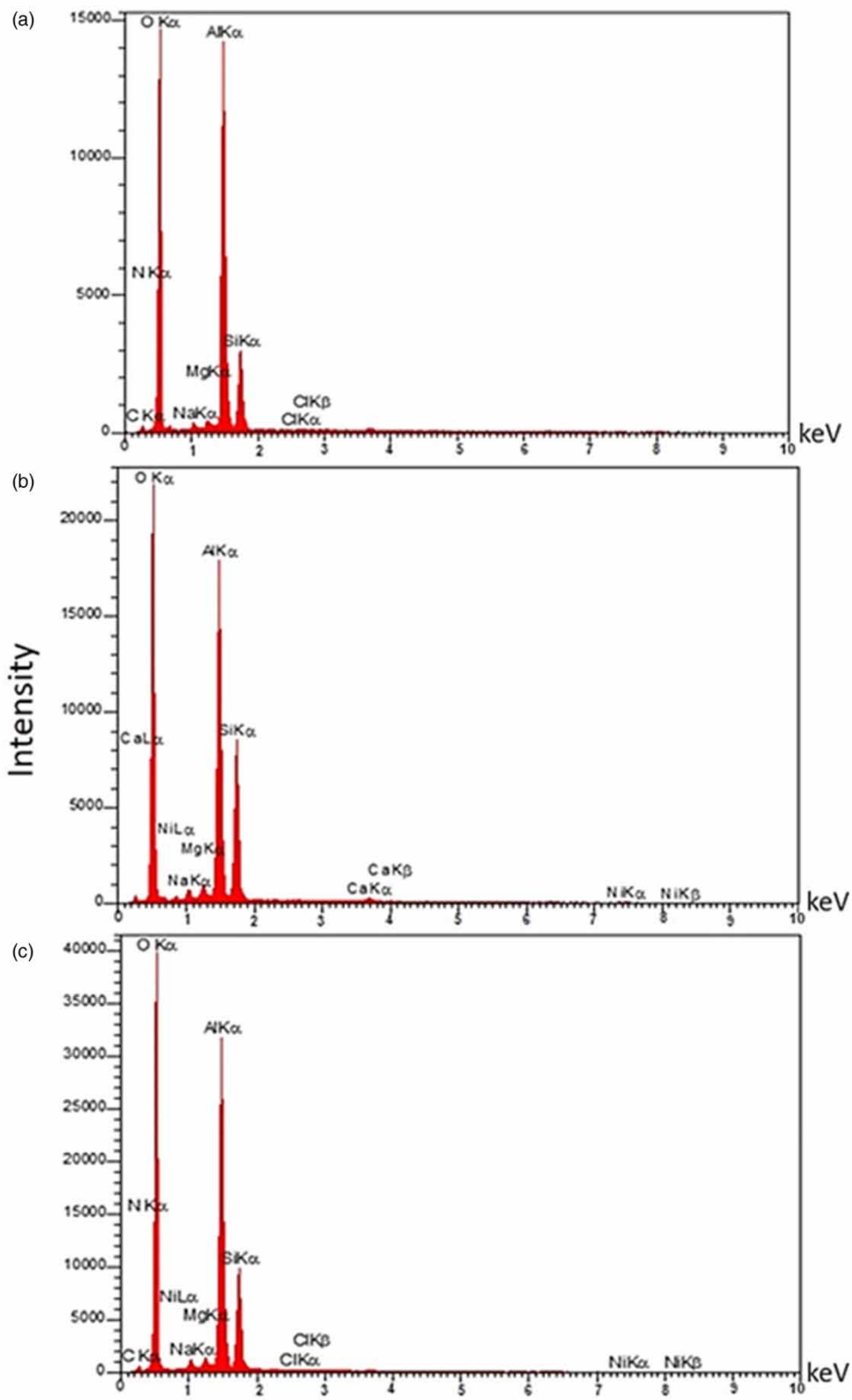

Figure 4 | EDX analysis of the modified nanoclay (a) after BO2 dye adsorption, (b) after Ni^{2+} adsorption, and (c) after BO2 dye and Ni^{2+} adsorption.

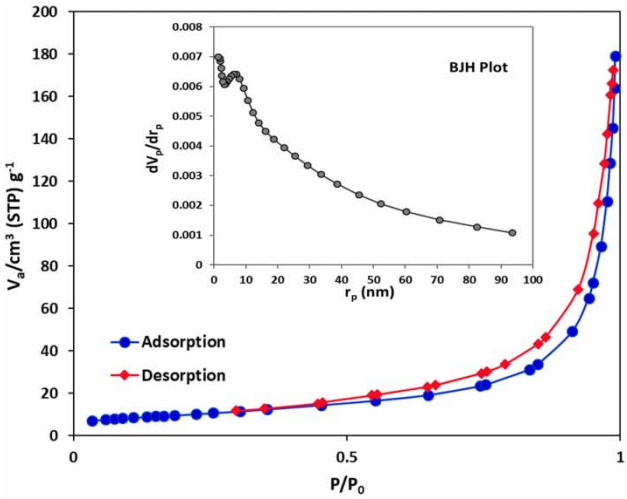

Figure 5 | N_2 adsorption–desorption isotherm of the adsorbent and the inset is displaying the BJH pore size distribution plot.

isotherm is related to capillary condensation taking place in mesopores and the initial part of this isotherm is associated with the monolayer–multilayer adsorption features and describes the strong interactions between the adsorbate and the adsorbent (Sing 1985). From the isotherm graph, at the high-pressure range (around $P/P_0 > 0.5$), the hysteresis loop has appeared and in the low relative pressure range, the adsorption and desorption lines coincide that can indicate the presence of the ink-bottle type of pores (Passe-Coutrin *et al.* 2008). The lower amounts of N_2 adsorbed at the low relative pressures demonstrated the presence of predominant mesopores in the adsorbent structure. Furthermore, the increase in the absorption at high relative pressure P/P_0 range (approximately approaching to 1.0) implied the existence of larger mesopores. As summarized in Table 2, the specific BET surface area of the nanoclay absorbent was found to be 35.6 $m^2 g^{-1}$ with a corresponding total pore volume of 0.2537 $cm^3 g^{-1}$ ($P/P_0 = 0.99$). Also, the mean pore diameter was obtained as 28.512 nm. The pore size distribution of the adsorbent obtained from the BJH method are presented in the inset of Figure 5. The BJH pore volume was 0.2585 $cm^3 g^{-1}$.

Table 2 | Calculated parameters of BET/BJH analysis for the adsorbent

Parameter	Measured value
BET surface area ($m^2 g^{-1}$)	35.6
Total pore volume ($P/P_0 = 0.99$) ($cm^3 g^{-1}$)	0.2537
Mean pore diameter (nm)	28.512
BJH pore volume ($cm^3 g^{-1}$)	0.2585

Dye adsorption studies

Effect of adsorbent dosage and contact time

Adsorbent dosage is one of the important parameters affecting the dye adsorption process and obtaining the optimum dosage is critical from two angles: (I) increasing the removal efficiency and (II) cost–effectiveness of the process from the economic viewpoint. For this purpose, the modified nanoclay adsorbent dosage was varied from 0.02 to 0.08 g L^{-1} while the other experimental parameters were constant (C_0: 10 mg L^{-1}, contact time: 30 min and temperature: 25 °C). The results are shown in Figure 6(b) that shows that the dye removal efficiency increased with increasing the adsorbent dose from 0.02 to 0.06 g L^{-1}. Increasing the adsorption efficiency with increasing adsorbent dose is due to the availability of more active sites of the adsorbent for the adsorption of dye molecules. However, as the adsorbent dose increased from 0.06 to 0.08 g L^{-1}, the removal efficiency decreased. Decreasing the adsorption efficiency with increasing adsorbent dose is due to the agglomeration of the nanoparticle adsorbents in solution, resulting in reduced active sites and accessible surfaces (Mahvi & Dalvand 2020). The reason for the agglomeration can be explained by the high surface energy of the nanomaterials (Zare *et al.* 2011). In fact, in a solution containing nanoparticle adsorbent, when the concentration of nanoparticle adsorbent increases from an optimal value, the surface energy contributes to agglomeration instead of leading to more dye removal. Eventually, the optimum amount of modified nanoclay for removing BO2 dye was selected as 0.06 g L^{-1} and used in further experiments.

Furthermore, it can be seen that the removal rate was very high during the initial moments of the process because there were many available active sites to adsorb the pollutant molecules. Afterward, the removal rate slowly reduced to reach the equilibrium due to an increase in surface coverage of the adsorbent. Based on this observation, the optimum contact time was found to be about 10 min; nevertheless, further experiments were performed up to 30 min, after which there is no significant uptake in the percentage of BO2 that was removed.

Effect of the alkaline surface modification of the adsorbent

To evaluate the effectiveness of the surface modification of nano-adsorbent, the efficiency of the raw and modified nanoclay for dye removal was assessed at the obtained optimum

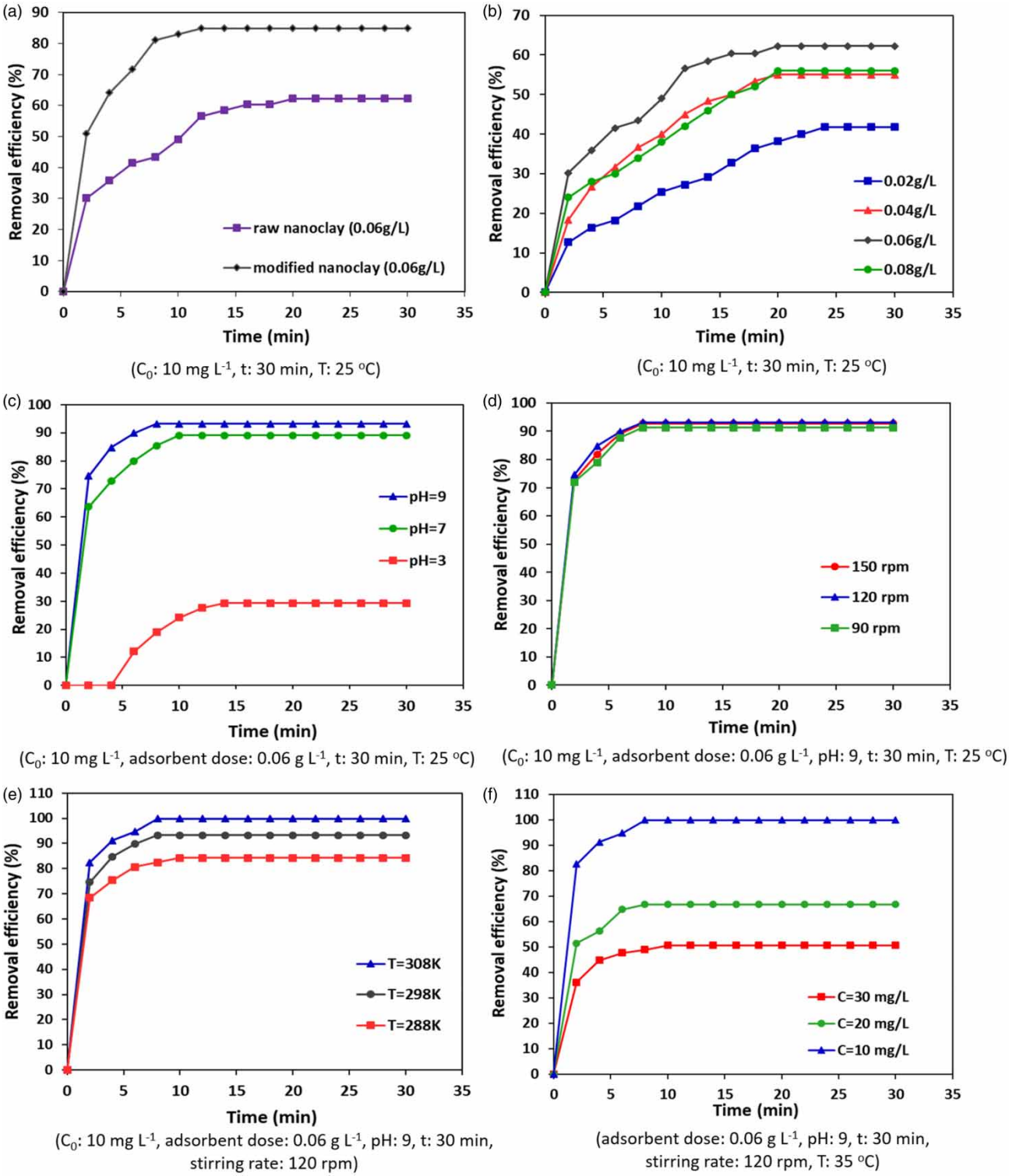

Figure 6 | (a) Effect of surface modification of the adsorbent on the removal efficiency of BO2 dye. Effect of (b) adsorbent dose, (c) pH, (d) stirring rate, (e) temperature, and (f) initial dye concentration on the removal efficiency of BO2 dye using alkaline-modified nanoclay adsorbent.

dose. For this purpose, in separate experiments, the solution was prepared according to the previous procedure and aforementioned conditions, and the amount of 0.06 g L^{-1} of raw and modified adsorbent was added to it. The results are presented in Figure 6(a) clearly showed the higher performance of the modified nanoclay adsorbent for BO2

dye removal, and the removal efficiency increased by about 23% after alkaline surface modification of the adsorbent. As a result, the modification of the inorganic surface of nanoclay adsorbent in the basic medium can create the hydroxide (OH^-) ions on the adsorbent active surfaces and then increase the adsorption of BO2 cationic dye due to the electrostatic attraction between the negative charges of adsorbent surface and positive charges of cationic BO2 dye.

Effect of pH

The pH of the sample solution is another critical parameter that affects the removal efficiency of the adsorbate in the adsorption process (Mahvi & Dalvand 2020). To investigate the effect of pH on the removal efficiency of BO2 dye, solutions were prepared at a concentration of 10 ppm at ambient temperature. The pH of the solutions was adjusted to 3, 7, and 9 using hydrochloric acid 1 M and sodium hydroxide 1 M, while the amount of modified nanoclay adsorbent and contact time were kept constant at 0.06 g L^{-1} and 30 min, respectively. The results (Figure 6(c)) indicated that the dye removal efficiency was significantly reduced in acidic conditions. The cause of this can be examined in two respects.

First, in the acidic medium, the amount of H^+ ions in the solution is increased. The H^+ ions and the cationic dye will compete for the adsorption on the free adsorption sites of the adsorbent surface. According to the smaller size of H^+ ions, it can be expected that this ion is successful in competition with the dye cation. Second, under acidic conditions, the adsorbent surface will be positive due to the presence of H^+ ions. Because of the electrostatic repulsion between these positive ions and the BO2 cationic dyes, the amount of adsorbed dye on the active surfaces of the adsorbent decreases (Sharma *et al.* 2016; Ehsan *et al.* 2017). The removal efficiency increased with the reduction of the acidity of the solution and reached to the maximum value (approximately 94%) in the alkaline medium. At high pH, OH^- ions are increased and may cover a portion of the active adsorption sites of the adsorbent surface. Then, the removal efficiency increased due to the electrostatic attraction between the adsorbent surface covered with the OH^- ions and the cationic adsorbate. As a result, the optimal pH value of 9 was selected for the following adsorption experiments.

Effect of stirring rate

Stirring can provide proper interactions between the adsorbate and adsorbent surface in the solution. Figure 6(d) illustrated the study regarding the influence of stirring rate on the dye removal efficiency, with rotation varying in 90, 120, and 150 rpm while the other parameters were kept constant (C_0: 10 mg L^{-1}, adsorbent dose: 0.06 g L^{-1}, contact time: 30 min, pH: 9 and temperature: 25 °C). It was found that there was no considerable increase in removal efficiency of BO2 dye by varying the stirring rate. However, the stirring rate of 120 rpm with a high removal efficiency of about 93% was chosen as the optimum value.

Effect of temperature

The effect of temperature was studied to investigate the influence of its changes on dye removal efficiency and calculate the thermodynamic parameters of the process. For this purpose, the adsorption experiments were carried out at three different temperatures of 288, 298 and 308 K under the optimized experimental parameters (C_0: 10 mg L^{-1}, adsorbent dose: 0.06 g L^{-1}, contact time: 30 min, pH: 9, and stirring rate: 120 rpm). It can be seen in Figure 6(e) that the removal efficiency has reached from 80% to 100% with increasing the temperature from 288 to 308 K. The enhancement of the removal efficiency with increasing the temperature may be related to the increasing the penetration of dye molecules inside mesopores of the nanoclay adsorbent at higher temperature as well as the high molecular mobility and in the result, increasing the contact between the adsorbent and adsorbate (Günay *et al.* 2013).

Effect of initial dye concentration

The adsorption process of BO2 dye in various initial concentrations of 10, 20 and 30 mg L^{-1} was performed under the optimized experimental variables (adsorbent dose: 0.06 g L^{-1}, pH: 9, contact time: 30 min, stirring rate: 120 rpm, and temperature: 35 °C). As the results indicated in Figure 6(f), the adsorbent capacity for dye adsorption decreased by increasing the initial dye concentration. After about 10 min of operation, dye removal decreased from 99.82% to 50.58% when dye concentration was increased from 10 to 30 mg L^{-1}. This can be attributed to the saturation of adsorption sites on the surface of the adsorbent. Indeed, by decreasing of dye concentration in the solution, the dye molecules have more chance to interact with the available sites on the modified nanoclay surface and, consequently, the adsorption rate is increased (Khan 2020).

After the investigation of the effect of different operational variables on dye removal efficiency, the adsorption of Ni^{2+} on the alkaline-modified nanoclay was studied. It

was exciting that under the optimized condition of the dye removal, the removal efficiency of 100% was obtained for the Ni^{2+}. All results and the corresponding Figure for the removal of Ni^{2+} by modified nanoclay are presented in Section 1 of the Supplementary Material.

Adsorption isotherms

Adsorption isotherms describe the interaction of the adsorbate with the adsorbent and present valuable information for interpreting the sorption mechanisms and surface characteristics of the adsorbent. In addition, the appropriate mathematical representation of the equilibrium isotherm based on an accurate adsorption mechanism is the most substantial part of designing the adsorption systems. In this study, adsorption isotherm experiments were carried out under the optimized experimental variables to find the most appropriate model that can describe the adsorption of BO2 dye onto modified nanoclay adsorbent. The adsorption equilibrium data were analyzed by the Langmuir (Langmuir 1916), and Freundlich (Freundlich 1906) models, and the linear fitting formulas of Langmuir and Freundlich adsorption isotherms are listed and described in Section 2 of the Supplementary Material. For the determination of standard deviation of the parameters in the isotherm models, we used a routine developed in Microsoft Excel (Comuzzi *et al.* 2003).

The correlation coefficient and adsorption constants of the Langmuir and Freundlich isotherms are summarized in Table 3. Also, the plots of adsorption isotherms are depicted in Figure 7. Based on the correlation coefficient (R^2) values, it can be concluded that the experimental data fitted well to the Langmuir isotherm ($R^2 = 0.9869$). This suggested the monolayer adsorption of BO2 dye onto the homogeneous surface of alkaline modified nanoclay. Furthermore, the obtained range of dimensionless constant separation factor R_L was between 0 and 1 (0.02–0.05), signifying that the adsorption process was favorable and the BO2 dye molecules can be easily adsorbed on the active sites of the modified nanoclay surface. The Langmuir monolayer adsorption capacity of modified nanoclay was estimated as 270 ± 7 mg g^{-1}.

Kinetics of adsorption

Adsorption kinetics explains the reaction rate between adsorbents and adsorbates and helps to predict the mechanism involved in sorption. In this research, the various kinds of kinetic models such as the pseudo-first-order (Lagergren 1898), pseudo-second-order (Ho 2006), and intra-particle

Table 3 | Isotherm parameters for the adsorption of BO2 onto modified nanoclay adsorbent

Langmuir isotherm[a]				Freundlich isotherm[a]		
R_L	K_L (L mg^{-1})	q_m (mg g^{-1})	R^2	1/n	K_F ($mg^{1-(1/n)}$ g^{-1} $L^{1/n}$)	R^2
(0.02–0.05) ±0.001	1.60 ± 0.08	270 ± 7	0.9869	0.053 ± 0.002	212 ± 25	0.8366

[a]These values are standard deviation at 95% confidence level.

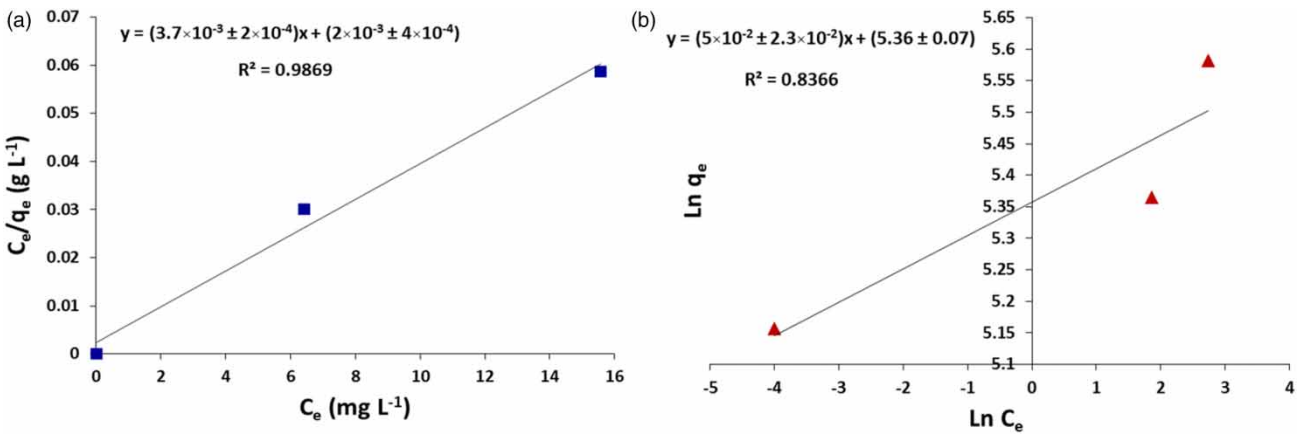

Figure 7 | (a) Langmuir and (b) Freundlich isotherm for the adsorption of BO2 dye onto modified nanoclay adsorbent.

diffusion (Weber & Morris 1963) were studied to investigate the mechanism of BO2 adsorption onto modified nanoclay adsorbent under the optimized experimental conditions. The details of the formulas of all three kinetic models are presented in Section 3 of the Supplementary Material. For the determination of standard deviation of the parameters in the kinetic models, we used a routine developed in Microsoft Excel (Comuzzi *et al.* 2003).

The diagrams for kinetic modeling are shown in Figure 8(a)–8(c). Also, the adsorption kinetic parameters of the models are presented in Table 4. It can be seen that compared with pseudo-first-order and intra-particle diffusion models, the pseudo-second-order was the best-fitted model to describe the kinetics of BO2 adsorption onto modified nanoclay with the high correlation coefficient of 0.9995. Looking at the experimental q_e ($q_{e,exp}$) and the model calculated q_e ($q_{e,cal}$) values, the $q_{e,cal}$ of the pseudo-second-order model was close to the $q_{e,exp}$, suggesting that the chemisorption was the rate-limiting step in the adsorption process. The pseudo-second-order kinetic rate constant (k_2) was 0.0105 ± 0.001 g mg^{-1} min^{-1}, testifying the rapid adsorption that can be attributed to more available

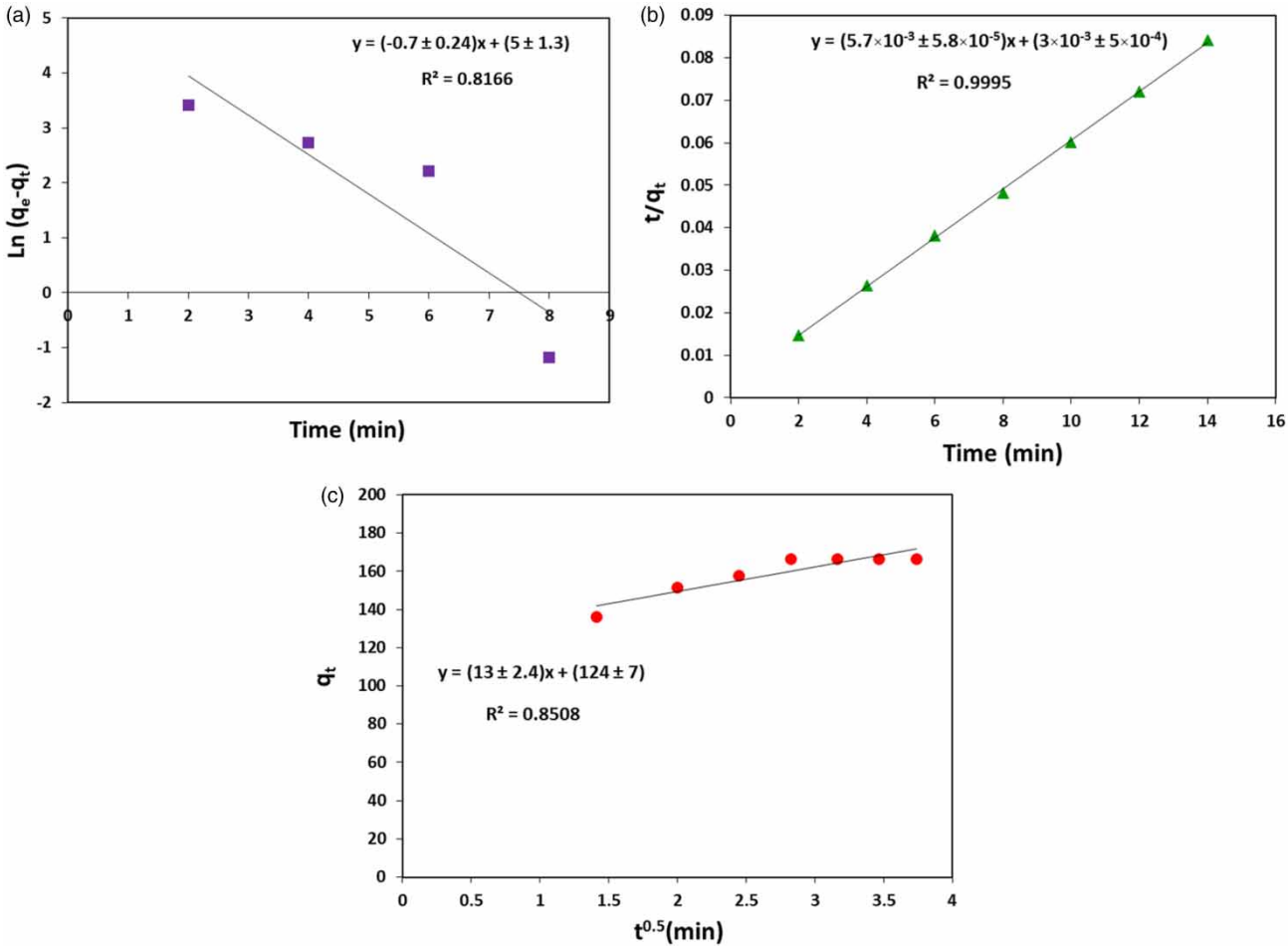

Figure 8 | The kinetic models describing the BO2 dye adsorption onto modified nanoclay adsorbent: (a) pseudo-first-order, (b) pseudo-second-order, and (c) intra-particle diffusion kinetic model.

Table 4 | Kinetics parameters for the adsorption of BO2 dye onto modified nanoclay

	Pseudo-first-order[a]			Pseudo-second-order[a]			Intra-particle diffusion[a]		
$q_{e,exp}$ (mg g^{-1})	$q_{e,cal}$ (mg g^{-1})	k_1 (min^{-1})	R^2	$q_{e,cal}$ (mg g^{-1})	k_2 (g mg^{-1} min^{-1})	R^2	k_{dif} (mg g^{-1} min$^{-0.5}$)	C (mg g^{-1})	R^2
166.7 ± 0.8	216 ± 35	0.7 ± 0.5	0.8166	175 ± 2	0.0105 ± 0.001	0.9995	13 ± 2.5	124 ± 15	0.8508

[a]These values are standard deviation at 95% confidence level.

Table 5 | Thermodynamic parameters for BO2 adsorption by modified nanoclay adsorbent

T (K)	ΔG (kJ mol^{-1})	ΔH (kJ mol^{-1})	ΔS (kJ mol^{-1} K^{-1})
288	−0.4	336 ± 15[a]	2 ± 1[a]
298	−12.0		
308	−23.7		

[a]These values are standard deviation at 95% confidence level.

sites for dye adsorption due to the alkaline modification of nanoclay surfaces. As can be observed from Figure 8(c), the regression was linear for the intra-particle diffusion model, but the plot did not pass through the origin demonstrating that the adsorption can be involved intra-particle diffusion process but that was not the rate-controlling step.

Thermodynamics of adsorption

The thermodynamic study helps to reach in-depth information about the energetic changes pertinent to the adsorption process and better understanding of temperature influence on the adsorption. To determine the thermodynamic parameters of the adsorption, including variations of the Gibbs free energy (ΔG), variations of the enthalpy (ΔH), and variations of the entropy (ΔS) and to study the nature of the adsorption process, the influence of temperature (288 – 308 K) on the adsorption was investigated (Seki & Yurdakoç 2006; Ehsan *et al.* 2017). The specific formulas of thermodynamics are provided in Section 4 of the Supplementary Material.

The thermodynamic parameters are listed in Table 5. The positive ΔH value confirmed the endothermic nature of the adsorption process of BO2 on the modified nanoclay surface. According to the obtained negative values for ΔG at different temperatures, it can be concluded that the nature of the adsorption process of BO2 onto the modified nanoclay is thermodynamically feasible and spontaneous. Moreover, the positive value of entropy change (ΔS) indicated the increased randomness at the modified nanoclay adsorbent-solution interface during the adsorption process.

CONCLUSIONS

In the present study, the available and cost-effective mineral material based on alkaline-modified nanoclay was directly used as an adsorbent to remove BO2 dye and Ni^{2+} from aqueous solutions. The effect of essential factors on the removal efficiency of BO2 dye such as adsorbent dose, contact time, pH, stirring speed, temperature and initial dye concentration were investigated and the optimum values for each of these variables with 100% efficiency were determined 0.06 g L^{-1}, 10 min, 9, 120 rpm, 35 °C and 10 mg L^{-1}, respectively. The Ni^{2+} was quantitatively removed at the same conditions of the BO2; therefore, it can be concluded that they can be removed simultaneously if they coexist in the solution. The equilibrium data showed the best fitting to Langmuir isotherm, which confirmed the monolayer coverage of the dye ions onto modified nanoclay surface. Kinetic studies showed that this process follows a pseudo-second-order kinetic model. Thermodynamic data also indicated that the aforementioned adsorption nature was endothermic and spontaneous. Overall, this study revealed that the modified nanoclay could be a potential candidate for removing BO2 dye and Ni^{2+} from an aqueous medium. More studies are needed for relevant and complex wastewater samples at pertinent pH values using industry-relevant nanoclay doses.

ACKNOWLEDGEMENTS

We would like to show our gratitude to the research councils of Arak Branch, Islamic Azad University, for their assistance during this research.

DATA AVAILABILITY STATEMENT

All relevant data are included in the paper or its Supplementary Information.

REFERENCES

Adeyemo, A. A., Adeoye, I. O. & Bello, O. S. 2017 Adsorption of dyes using different types of clay: a review. *Applied Water Science* **7** (2), 543–568.

Alexandre, M. & Dubois, P. 2000 Polymer-layered silicate nanocomposites: preparation, properties and uses of a new class of materials. *Materials Science and Engineering: R: Reports* **28** (1–2), 1–63.

Almeida, C., Debacher, N., Downs, A., Cottet, L. & Mello, C. 2009 Removal of methylene blue from colored effluents by adsorption on montmorillonite clay. *Journal of Colloid and Interface Science* **332** (1), 46–53.

Anirudhan, T. & Ramachandran, M. 2015 Adsorptive removal of basic dyes from aqueous solutions by surfactant modified bentonite clay (organoclay): kinetic and competitive adsorption isotherm. *Process Safety and Environmental Protection* **95**, 215–225.

Auta, M. & Hameed, B. 2012 Modified mesoporous clay adsorbent for adsorption isotherm and kinetics of methylene blue. *Chemical Engineering Journal* **198**, 219–227.

Banerjee, S., Sharma, G. C., Chattopadhyaya, M. & Sharma, Y. C. 2014 Kinetic and equilibrium modeling for the adsorptive removal of methylene blue from aqueous solutions on of activated fly ash (AFSH). *Journal of Environmental Chemical Engineering* **2** (3), 1870–1880.

Batista, A., Melo, V. & Gilkes, R. 2017 Scanning and transmission analytical electron microscopy (STEM-EDX) identifies minor minerals and the location of minor elements in the clay fraction of soils. *Applied Clay Science* **135**, 447–456.

Beyene, H. D. 2014 The potential of dyes removal from textile wastewater by using different treatment technology. A review. *International Journal of Environmental Monitoring and Analysis* **2** (6), 347–353.

Cempel, M. & Nikel, G. 2006 Nickel: a review of its sources and environmental toxicology. *Polish Journal of Environmental Studies* **15** (3), 375–382.

Comuzzi, C., Polese, P., Melchior, A., Portanova, R. & Tolazzi, M. 2003 SOLVERSTAT: a new utility for multipurpose analysis. An application to the investigation of dioxygenated Co(II) complex formation in dimethylsulfoxide solution. *Talanta* **59** (1), 67–80.

Djomgoue, P. & Njopwouo, D. 2013 FT-IR spectroscopy applied for surface clays characterization. *Journal of Surface Engineered Materials and Advanced Technology* **3** (04), 275.

Ehsan, A., Bhatti, H. N., Iqbal, M. & Noreen, S. 2017 Native, acidic pre-treated and composite clay efficiency for the adsorption of dicationic dye in aqueous medium. *Water Science and Technology* **75** (4), 753–764.

El-Geundi, M. S. 1997 Adsorbents for industrial pollution control. *Adsorption Science & Technology* **15** (10), 777–787.

El Haouti, R., Ouachtak, H., El Guerdaoui, A., Amedlous, A., Amaterz, E., Haounati, R., Addi, A. A., Akbal, F., El Alem, N. & Taha, M. L. 2019 Cationic dyes adsorption by Na-Montmorillonite Nano Clay: experimental study combined with a theoretical investigation using DFT-based descriptors and molecular dynamics simulations. *Journal of Molecular Liquids* **290**, 111139.

Fil, B. A., Özmetin, C. & Korkmaz, M. 2014 Characterization and electrokinetic properties of montmorillonite. *Bulgarian Chemical Communications* **46** (2), 258–263.

Freundlich, H. 1906 Over the adsorption in solution. *Journal of Physical Chemistry* **57** (385471), 1100–1107.

Gamoudi, S. & Srasra, E. 2019 Adsorption of organic dyes by $HDPy^{+}$-modified clay: effect of molecular structure on the adsorption. *Journal of Molecular Structure* **1193**, 522–531.

Gunatilake, S. 2015 Methods of removing heavy metals from industrial wastewater. *Methods* **1** (1), 14.

Günay, A., Ersoy, B., Dikmen, S. & Evcin, A. 2013 Investigation of equilibrium, kinetic, thermodynamic and mechanism of Basic Blue 16 adsorption by montmorillonitic clay. *Adsorption* **19** (2–4), 757–768.

Haddad, M., Abid, S., Hamdi, M. & Bouallagui, H. 2018 Reduction of adsorbed dyes content in the discharged sludge coming from an industrial textile wastewater treatment plant using aerobic activated sludge process. *Journal of Environmental Management* **223**, 936–946.

Hajiaghababaei, L., Abozari, S., Badiei, A., Zarabadi Poor, P., Dehghan Abkenar, S., Ganjali, M. R. & Mohammadi Ziarani, G. 2017 Amino ethyl-functionalized SBA-15: a promising adsorbent for anionic and cationic dyes removal. *Iranian Journal of Chemistry and Chemical Engineering (IJCCE)* **36** (1), 97–108.

Hassani, A., Soltani, R. D. C., Kıranşan, M., Karaca, S., Karaca, C. & Khataee, A. 2016 Ultrasound-assisted adsorption of textile dyes using modified nanoclay: central composite design optimization. *Korean Journal of Chemical Engineering* **33** (1), 178–188.

Hisada, M., Tomizawa, Y. & Kawase, Y. 2019 Removal kinetics of cationic azo-dye from aqueous solution by poly-γ-glutamic acid biosorbent: contributions of adsorption and complexation/precipitation to Basic Orange 2 removal. *Journal of Environmental Chemical Engineering* **7** (3), 103157.

Ho, Y.-S. 2006 Review of second-order models for adsorption systems. *Journal of Hazardous Materials* **136** (3), 681–689.

Jiang, J.-Q. & Ashekuzzaman, S. 2012 Development of novel inorganic adsorbent for water treatment. *Current Opinion in Chemical Engineering* **1** (2), 191–199.

Khan, M. 2020 Adsorption of methylene blue onto natural Saudi Red Clay: isotherms, kinetics and thermodynamic studies. *Materials Research Express* **7**, 055507.

Khataee, A., Dehghan, G., Zarei, M., Fallah, S., Niaei, G. & Atazadeh, I. 2013 Degradation of an azo dye using the green macroalga *Enteromorpha* sp. *Chemistry and Ecology* **29** (3), 221–233.

Kumar, K. Y., Muralidhara, H., Nayaka, Y. A., Balasubramanyam, J. & Hanumanthappa, H. 2013 Low-cost synthesis of metal oxide nanoparticles and their application in adsorption of commercial dye and heavy metal ion in aqueous solution. *Powder Technology* **246**, 125–136.

Lagergren, S. K. 1898 About the theory of so-called adsorption of soluble substances. *Sven. Vetenskapsakad. Handingarl* **24**, 1–39.

Langmuir, I. 1916 The constitution and fundamental properties of solids and liquids. Part I. Solids. *Journal of the American Chemical Society* **38** (11), 2221–2295.

Li, F., Huang, J., Xia, Q., Lou, M., Yang, B., Tian, Q. & Liu, Y. 2018 Direct contact membrane distillation for the treatment of industrial dyeing wastewater and characteristic pollutants. *Separation and Purification Technology* **195**, 83–91.

Mahdavinia, G. R., Massoumi, B., Jalili, K. & Kiani, G. 2012 Effect of sodium montmorillonite nanoclay on the water absorbency and cationic dye removal of carrageenan-based nanocomposite superabsorbents. *Journal of Polymer Research* **19** (9), 1–13.

Mahvi, A. H. & Dalvand, A. 2020 Kinetic and equilibrium studies on the adsorption of Direct Red 23 dye from aqueous solution using montmorillonite nanoclay. *Water Quality Research Journal* **55** (2), 132–144.

Malayoglu, U. 2018 Removal of heavy metals by biopolymer (chitosan)/nanoclay composites. *Separation Science and Technology* **53** (17), 2741–2749.

Mezohegyi, G., van der Zee, F. P., Font, J., Fortuny, A. & Fabregat, A. 2012 Towards advanced aqueous dye removal processes: a short review on the versatile role of activated carbon. *Journal of Environmental Management* **102**, 148–164.

Murray, H. H. 2000 Traditional and new applications for kaolin, smectite, and palygorskite: a general overview. *Applied Clay Science* **17** (5–6), 207–221.

Nazir, M. S., Kassim, M. H. M., Mohapatra, L., Gilani, M. A., Raza, M. R. & Majeed, K. 2016 Characteristic properties of nanoclays and characterization of nanoparticulates and nanocomposites. In: *Nanoclay Reinforced Polymer Composites* (M. Jawaid, A. Qaiss & R. Bouhfid, eds). Springer, Singapore, pp. 35–55.

Ong, S., Lee, C. & Zainal, Z. 2007 Removal of basic and reactive dyes using ethylenediamine modified rice hull. *Bioresource Technology* **98** (15), 2792–2799.

Ouaddari, H., Karim, A., Achiou, B., Saja, S., Aaddane, A., Bennazha, J., El Hassani, I. E. A., Ouammou, M. & Albizane, A. 2019 New low-cost ultrafiltration membrane made from purified natural clays for direct Red 80 dye removal. *Journal of Environmental Chemical Engineering* **7** (4), 103268.

Öztürk, A. & Malkoc, E. 2014 Adsorptive potential of cationic Basic Yellow 2 (BY2) dye onto natural untreated clay (NUC) from aqueous phase: mass transfer analysis, kinetic and equilibrium profile. *Applied Surface Science* **299**, 105–115.

Padmesh, T., Vijayaraghavan, K., Sekaran, G. & Velan, M. 2005 Batch and column studies on biosorption of acid dyes on fresh water macro alga *Azolla filiculoides*. *Journal of Hazardous Materials* **125** (1–3), 121–129.

Park, Y., Ayoko, G. A. & Frost, R. L. 2011 Application of organoclays for the adsorption of recalcitrant organic molecules from aqueous media. *Journal of Colloid and Interface Science* **354** (1), 292–305.

Passe-Coutrin, N., Altenor, S., Cossement, D., Jean-Marius, C. & Gaspard, S. 2008 Comparison of parameters calculated from the BET and Freundlich isotherms obtained by nitrogen adsorption on activated carbons: a new method for calculating the specific surface area. *Microporous and Mesoporous Materials* **111** (1–3), 517–522.

Pimol, P., Khanidtha, M. & Prasert, P. 2008 Influence of particle size and salinity on adsorption of basic dyes by agricultural waste: dried Seagrape (*Caulerpa lentillifera*). *Journal of Environmental Sciences* **20** (6), 760–768.

Qamar, M., Saquib, M. & Muneer, M. 2005 Semiconductor-mediated photocatalytic degradation of anazo dye, chrysoidine Y in aqueous suspensions. *Desalination* **171** (2), 185–193.

Rao, R. A. K. & Kashifuddin, M. 2016 Adsorption studies of Cd (II) on ball clay: comparison with other natural clays. *Arabian Journal of Chemistry* **9**, S1233–S1S41.

Ren, X., Zhang, Z., Luo, H., Hu, B., Dang, Z., Yang, C. & Li, L. 2014 Adsorption of arsenic on modified montmorillonite. *Applied Clay Science* **97**, 17–23.

Salam, M. A., Kosa, S. A. & Al-Beladi, A. A. 2017 Application of nanoclay for the adsorptive removal of Orange G dye from aqueous solution. *Journal of Molecular Liquids* **241**, 469–477.

Salleh, M. A. M., Mahmoud, D. K., Karim, W. A. W. A. & Idris, A. 2011 Cationic and anionic dye adsorption by agricultural solid wastes: a comprehensive review. *Desalination* **280** (1–3), 1–13.

Seki, Y. & Yurdakoç, K. 2006 Adsorption of promethazine hydrochloride with KSF montmorillonite. *Adsorption* **12** (1), 89–100.

Senthilkumaar, S., Varadarajan, P., Porkodi, K. & Subbhuraam, C. 2005 Adsorption of methylene blue onto jute fiber carbon: kinetics and equilibrium studies. *Journal of Colloid and Interface Science* **284** (1), 78–82.

Sharifi, A., Montazerghaem, L., Naeimi, A., Abhari, A. R., Vafaee, M., Ali, G. A. & Sadegh, H. 2019 Investigation of photocatalytic behavior of modified ZnS:Mn/MWCNTs nanocomposite for organic pollutants effective photodegradation. *Journal of Environmental Management* **247**, 624–632.

Sharma, P., Borah, D. J., Das, P. & Das, M. R. 2016 Cationic and anionic dye removal from aqueous solution using montmorillonite clay: evaluation of adsorption parameters and mechanism. *Desalination and Water Treatment* **57** (18), 8372–8388.

Sing, K. S. 1985 Reporting physisorption data for gas/solid systems with special reference to the determination of surface area and porosity (Recommendations 1984). *Pure and Applied Chemistry* **57** (4), 603–619.

Soltani, R. D. C., Khataee, A., Safari, M. & Joo, S. 2013 Preparation of bio-silica/chitosan nanocomposite for adsorption of a textile dye in aqueous solutions. *International Biodeterioration & Biodegradation* **85**, 383–391.

Uddin, M. K. 2017 A review on the adsorption of heavy metals by clay minerals, with special focus on the past decade. *Chemical Engineering Journal* **308**, 438–462.

Vanamudan, A. & Pamidimukkala, P. 2015 Chitosan, nanoclay and chitosan–nanoclay composite as adsorbents for Rhodamine-6G and the resulting optical properties. *International Journal of Biological Macromolecules* **74**, 127–135.

Wang, X., Jiang, C., Hou, B., Wang, Y., Hao, C. & Wu, J. 2018 Carbon composite lignin-based adsorbents for the adsorption of dyes. *Chemosphere* **206**, 587–596.

Weber, W. J. & Morris, J. C. 1963 Kinetics of adsorption on carbon from solution. *Journal of the Sanitary Engineering Division* **89** (2), 31–60.

Xiao, J., Xie, Y. & Cao, H. 2015 Organic pollutants removal in wastewater by heterogeneous photocatalytic ozonation. *Chemosphere* **121**, 1–17.

Yagub, M. T., Sen, T. K., Afroze, S. & Ang, H. M. 2014 Dye and its removal from aqueous solution by adsorption: a review. *Advances in Colloid and Interface Science* **209**, 172–184.

Zare, Y., Garmabi, H. & Sharif, F. 2011 Optimization of mechanical properties of PP/Nanoclay/$CaCO_3$ ternary nanocomposite using response surface methodology. *Journal of Applied Polymer Science* **122** (5), 3188–3200.

Zhu, S., Xia, M., Chu, Y., Khan, M. A., Lei, W., Wang, F., Muhmood, T. & Wang, A. 2019 Adsorption and desorption of Pb(II) on L-lysine modified montmorillonite and the simulation of interlayer structure. *Applied Clay Science* **169**, 40–47.

First received 7 January 2021; accepted in revised form 18 March 2021. Available online 29 March 2021